Understanding Gold−Thiolate Cluster Emission from Self-assembled Monolayers upon Kiloelectronvolt Ion Bombardment

B. Arezki,[†] A. Delcorte,*[,†] B. J. Garrison,[‡] and P. Bertrand[†]

Université Catholique de Louvain, PCPM, Croix du Sud, 1-B1348 Louvain-la-Neuve, Belgium, and Department of Chemistry, 104 Chemistry Building, The Pennsylvania State University, University Park, Pennsylvania 16802

Received: September 14, 2005; In Final Form: December 23, 2005

This article focuses on the emission of organometallic clusters upon kiloelectronvolt ion bombardment of self-assembled monolayers. It is particularly relevant for the elucidation of the physical processes underlying secondary ion mass spectrometry (SIMS). The experimental system, an overlayer of octanethiols on gold, was modeled by classical molecular dynamics, using a hydrocarbon potential involving bonding and nonbonding interactions (AIREBO). To validate the model, the calculated mass and energy distributions of sputtered atoms and molecules were compared to experimental data. Our key finding concerns the emission mechanism of large clusters of the form M_xAu_y up to M_6Au_5 (where M is the thiolate molecule), which were not observed under sub-kiloelectronvolt projectile bombardment. Statistically, they are predominantly formed in high-yield events, where many atoms, fragments, and (supra)molecular species are desorbed from the surface. From the microscopic viewpoint, these high-yield events mostly stem from the confinement of the projectile and recoil atom energies in a finite microvolume of the sample surface. As a result of the high local energy density, molecular aggregates desorb from an overheated liquidlike region surrounding the impact point of the projectile.

1. Introduction

Static secondary ion mass spectrometry (SIMS) is a surface analysis technique with a very large spectrum of application fields, including, for example, geology, materials science, biology, and medecine.[1] To pursue the performance improvement (smarter projectiles, enhanced sample preparation procedures) and refine the quality of the data interpretation in organic SIMS, a good understanding of molecular desorption is necessary.[2] This, however, is a challenging task, because the mechanisms of polyatomic particle sputtering are complex and many-body in nature. For instance, the desorption of fragile (bio)molecules following the impact of particles with energies exceeding largely those of chemical bonds is, at first sight, a surprising and even counter-intuitive observation. Unraveling such, and other, effects is the key to controlling the relevant parameters of (supra)molecular emission from organic samples. In practice, analytical models can explain relatively "simple" sputtering results,[3] but they cannot treat the sequence of many-body interactions leading to the emission of complex polyatomic ensembles. For this purpose, classical molecular dynamics (MD) has now proved to be the method of choice.

Thin organic overlayers have been widely investigated using MD simulations. Several studies explain desorption from physisorbed layers including small molecules and polymers on metals.[4−9] However, only a few reports have been devoted to the understanding of particle-induced desorption from chemisorbed systems, where molecules are strongly bound to the substrate.[10−12] Self-assembled monolayers (SAMs) constitute good models of those systems because their structure and properties have been characterized by a variety of analytical techniques over the years.[13] One specific effect observed upon energetic ion bombardment of strongly bound molecules is the emission of large numbers of organometallic clusters, M_xMe_y, where M represents the organic molecule and Me the metal atom. The explanation of this effect remains elusive, especially for large clusters with more than 3−4 constituents.

Among the experimental studies carried out to explain sputtering from SAMs,[14−19] little is said concerning the origin of the M_xMe_y cluster ions observed in the SIMS mass spectra. The first hypotheses were proposed by Tarlov et al. in their pioneering study of various alkanethiols ($CH_3(CH_2)_nSH$) on gold, under Ar^+ kiloelectronvolt bombardment.[15] The authors suggested that a recombination reaction could explain the formation of M_2Au^- ($M = CH_3(CH_2)_nS$), the largest cluster ion they observed at that time. A similar aggregation process has been proposed recently in another ToF-SIMS study to explain the emission of higher mass gold−thiolate cluster ions.[18] In our previous experimental contributions, the kinetic energy distributions (KEDs) of gold−thiolate cluster ions have shown that collisional processes are involved in their emission.[20−22] Moreover, the metastable decay of M_xAu_y clusters in the acceleration section of the spectrometer has been demonstrated, indicating that other processes besides just recombination influence the measured mass distributions of clusters. Concerning the specific processes leading to cluster formation in the surface region, however, experimental methods such as SIMS and SNMS may provide some pieces of the puzzle but not the complete explanation. From the theoretical viewpoint, Liu et al. have reported the results of a detailed MD study involving alkanethiols on gold under 700 eV Ar bombardment.[10−12] In their

* To whom correspondence should be addressed. Tel: 3210473582. Fax: 3210473452. E-mail: delcorte@pcpm.ucl.ac.be.
[†] Université Catholique de Louvain.
[‡] The Pennsylvania State University.

10.1021/jp058252f CCC: $33.50
Published on Web 03/10/2006

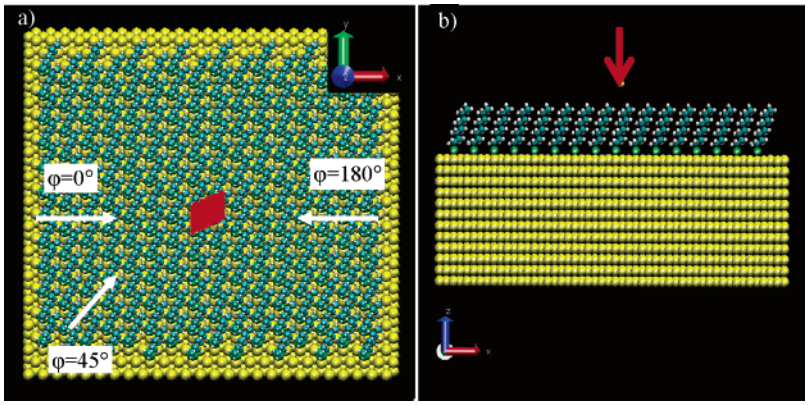

Figure 1. Equilibrium configuration of the octanethiol/Au sample used to model 8 keV Ar bombardment. Au atoms are represented by large yellow spheres, S atoms by green spheres, and C and H atoms by blue and smaller white spheres, respectively. (a) Top view of the sample. The impact area is indicated by a red lozenge, and some values of the chosen azimuthal angles φ are indicated by white arrows. (b) Side view of the sample. The projectile is represented for $\varphi = 90°$ by a red arrow.

investigation, the authors suggest the concept of a precursor cluster for the formation of larger M_xAu_y aggregates. Their simulations show that the precursor originates from the recombination between a gold atom and an alkanethiolate molecule in the "selvedge" layer of the surface. The precursor MAu cluster recombines then with other Au or M to form larger aggregates. In the detailed investigation carried out in that work, only low-mass clusters have been observed. This is most probably due to the low projectile energy, as was also suggested by the experiments of Tarlov et al.[15] A complementary study on this topic, involving more energetic projectiles, was judged necessary to compare with our experimental data, where large clusters have been observed.

The main goal of this study is to elucidate the mechanism of M_xAu_y cluster emission from SAMs, for a projectile energy that is relevant with respect to SIMS (5−25 keV). For this purpose, we use a combination of SIMS analysis and realistic MD simulations. The novelty of the presented simulations lies in the projectile energy range (an order of magnitude larger than refs 10−12) and the use of a more realistic potential, including long-range forces between the hydrocarbon chains of the alkanethiols. This second feature appears necessary for a correct description of clusters involving several molecules. As shown in the results, a good agreement is achieved between the experimental and calculated mass and energy distributions. Further processing of our MD results provides us with a microscopic understanding of the emission processes. For instance, it is found that M_xAu_y clusters eject predominantly in high-sputtering-yield events, via a late process. Their emission often starts from the overheated liquidlike region created in the gold crystal as a result of the high energy density deposited by the collision cascade.

2. Material and Methods

2.1. MD Simulations. MD computer simulation has been described extensively elsewhere.[7] This method consists of integrating Hamilton's equations of motion in order to obtain the positions and velocities of all the atoms in the system, as a function of time. From the final positions and velocities of the ejected species, various properties are determined such as their mass and kinetic energy distributions. Also, mechanistic information regarding sputtering can be obtained by analyzing individual trajectories.

For the 8 keV Ar bombardment of SAMs of octanethiol on Au(111), we designed a larger adsorbate/Au system than that used by Liu et al. in ref 12, to contain most of the collisional events. The gold substrate was a finite microcrystallite containing 8736 Au atoms in 12 layers of 728 atoms each. The calculations were initialized by placing a total of 192 octanethiolates, $CH_3(CH_2)_7S$, on the 3-fold sites of the Au(111) substrate in a $(\sqrt{3} \times \sqrt{3})R30°$ arrangement. Prior to Ar atom impact, the entire system was relaxed to a minimum energy configuration using periodic boundary conditions. The Ar atoms were directed along a polar angle $\theta = 45°$ at different azimuthal angles φ (Figure 1). A total of 1200 trajectories have been calculated. At the end of the trajectories, the ejected clusters were identified after evaluating the total internal energy of the groups of linked pairs of atoms constituting the ejected species. If this energy was less than zero, then the group of atoms was counted as an ejected cluster.

A set of empirical pairwise and many-body potentials has been used to describe the interactions between the different atoms in the system. Briefly, the projectile interacted with the rest of the atoms via a purely repulsive Molière potential. The Au−Au interactions were described by the molecular dynamics/Monte Carlo corrected effective medium (MD/MC-CEM) potential.[23] A Morse potential accounted for the S−S and S−C interactions, whereas Lennard-Jones potential functions were used for the S−H, Au−C, and Au−H interactions. In the particular case of the Au−S bond, a modified Morse potential was used to better describe the Au−thiolate clusters. In this potential, the energy parameter of the conventional Morse potential D_e varies as a function of the height of the Au−S pair above the surface.[12] Of special interest in this work was the use of the adaptive intermolecular potential, AIREBO, developed by Stuart et al.[24] for hydrocarbons. This potential introduced a long-range part within the original REBO potential,[25] accounting for van der Waals interactions between the thiolate chains.

2.2. ToF-SIMS Experiments. The studied molecules were octanethiols $CH_3(CH_2)_7SH$ (>98%, Aldrich). The SAMs were prepared on gold films evaporated onto silicon substrates. The metallization was carried out in an Edwards evaporator. The Si wafers, cleaned with 2-propanol, were first primed with a 5 nm adhesive layer of titanium (0.1 nm/s at $\sim 10^{-6}$ mbar); a 100 nm Au layer was then deposited in the same conditions. The Au/Ti/Si surfaces were immediately immersed in a 1 mM fresh solution of alkanethiols diluted in absolute ethanol. After immersion during ~24 h, the samples were thoroughly rinsed in absolute ethanol, dried with a stream of N_2 gas, and directly transferred into the vacuum system for SIMS analysis.

The experimental setup and the KED measurement procedure have been already described in detail elsewhere.[26,27] Briefly,

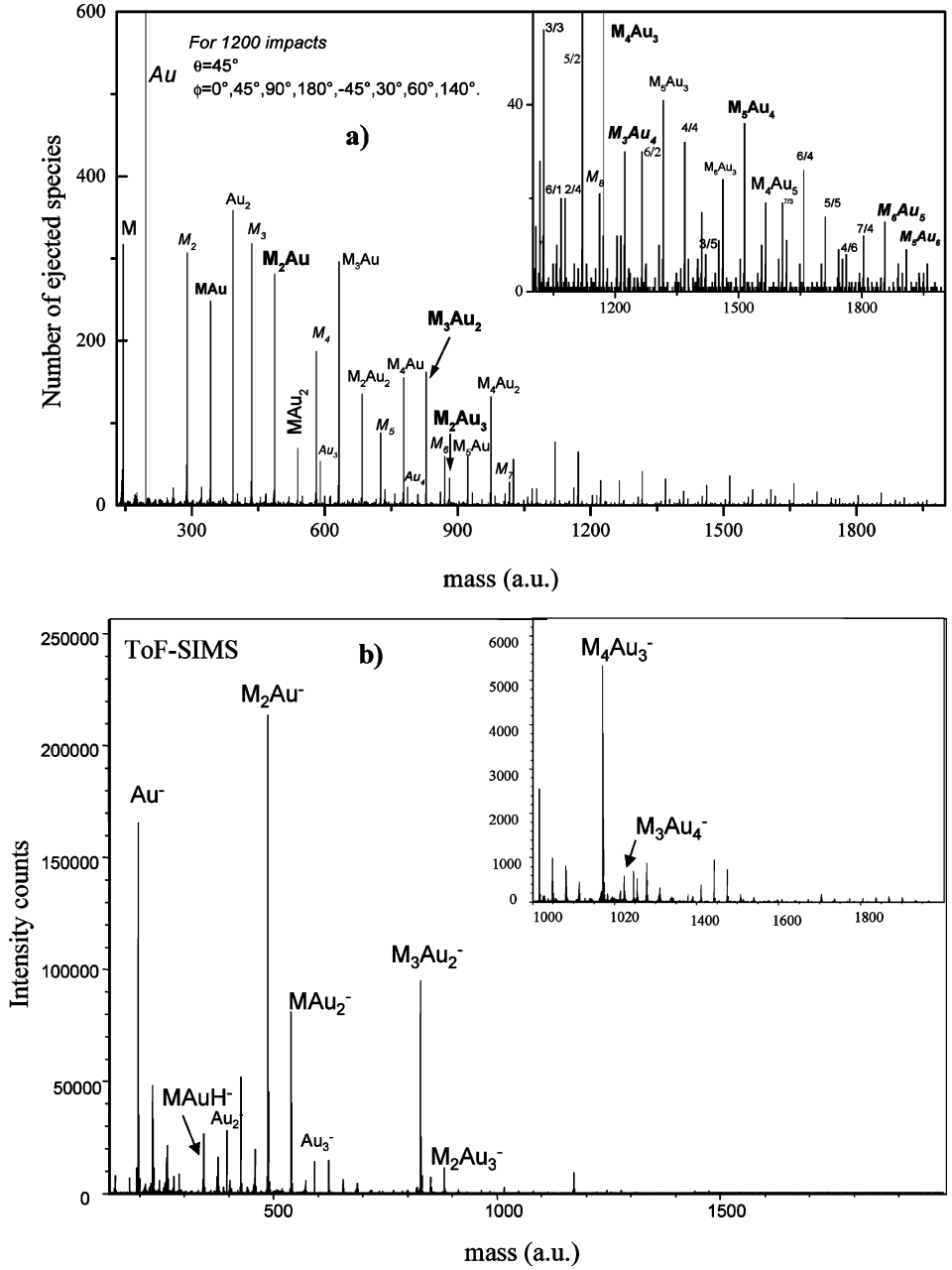

Figure 2. Comparison between the mass distributions of sputtered species obtained from MD simulations of octanethiol/Au under 8 keV Ar bombardment (a) and from ToF-SIMS under 15 keV Ga^+ bombardment (b).

the mass spectra and the KEDs were obtained in a PHI-EVANS time-of-flight secondary ion mass microscope/ microprobe using a (8 kHz) pulsed 15 keV $^{69}Ga^+$ beam (550 pA DC current, 2 ns pulse width after electrodynamic bunching).[28] The primary ion beam was focused (0.2 μm) and rastered onto a 120 μm × 120 μm area. The secondary ions, accelerated by a 3 kV potential applied on the sample, were post-accelerated before reaching the detector (7 kV). The different energy windows were selected owing to a slit (1.5 eV passband) placed at the crossover following the first electrostatic analyzer. With this procedure, about 40 mass spectra were recorded in the mass range 0−2000 Da during 300 s acquisition time (1.3×10^{12} ions/cm^2/spectrum). During these experiments, a fresh area was bombarded for each energy window, to avoid degradation effects.

3. Results and Discussion

The results are divided in three sections. First, the similarities and differences between the MD simulations and the ToF-SIMS experiment are explored and interpreted. In the second part of the results, a general view of cluster emission from SAMs is established, through the analysis of the statistics provided by the model. Finally, we present a microscopic study of trajectories representative of low and high emission events, respectively. A discussion of the results and a comparison to previous reports (when they are available) are proposed in each section.

3.1. SIMS Observations vs Molecular Dynamics. The first step of our study was to identify the gold−thiolate clusters ejected from the octanethiol assembly in the model and to compare these species to the mass distribution obtained in ToF-SIMS. In the calculated mass spectrum, there are a large number of peaks corresponding to M_xAu_y clusters with various x/y combinations up to M_5Au_6 (Figure 2a). Among the obtained aggregates, almost all the $M_xAu_{x\pm1}$ are observed experimentally as negative ions, including M_2Au^-, MAu_2^-, $M_3Au_2^-$, $M_2Au_3^-$, $M_4Au_3^-$, and even $M_3Au_4^-$ with a very low intensity (Figure 2b). Clusters with other x/y combinations are observed only in

the MD spectra. The simulations also predict intense peaks corresponding to thiolate clusters M_x that are not observed experimentally.

As shown in Figure 2, there are differences between the MD results and the experiment. Some of these might be due to the potentials used in the simulation. In particular, the Au−S interaction is described by a pair potential with a well depth varying with the height above the sample surface. By design, it is not expected to account for the energetics of large clusters as precisely as that of the M−Au pair.[12] Other differences should also arise from ionization processes required for SIMS analysis. As mentioned in the Experimental Section, ionization and charge exchange processes are absent from the model because of its classical nature. Despite these expected differences, one remarkable similarity is the extent of the mass distribution that is comparable in the model and the experiment. The large clusters appearing in the mass distribution of Figure 2 have not been reported in the simulations of Liu et al.[12] This effect can be explained by the much lower projectile energy used in their study (700 eV). In this respect, it is noteworthy that high-mass clusters have been observed by Tarlov et al.[15] in the mass spectra of octanethiols/Au for 7 keV Xe^+ bombardment but not for 500 eV Xe^+ bombardment. The authors suggested that the ejection of bigger aggregates was the consequence of the larger amount of energy transferred to the metal, which is confirmed and explained in detail by the MD simulations (see section 3.3).

The kinetic energy distributions provide more specific information about the emission mechanisms. In Figure 3, the calculated energy distributions of Au, M, and M_2Au are plotted along with those measured experimentally. To compare with the experimental data, the calculated energy spectra have been convoluted with an energy passband of 1.5 eV, similar to the experimental value. In general, the results show that the energy spectra predicted by the MD reasonably match the shape and the peak position of the experimental curves. In the case of M_2Au, a divergence from the experimental spectrum is observed for energies exceeding 4 eV (Figure 3c). This difference could be due either to the ionization mechanism or to the delayed dissociation of large aggregates. Delayed unimolecular processes are not described in the model because they would require very long calculation times and, possibly, more accurate potentials. ToF-SIMS measurements, however, demonstrate that unimolecular dissociation of excited gold−thiolate clusters takes place during their flight to the detector.[21,22] To explore this possibility within the model, one can check the stability of the ejected particles using their internal energy. In principle, the internal energy of an ejected species should be compared to a sensible energy threshold for unimolecular dissociation.[5] If it is larger than the threshold, then the polyatomic species is expected to dissociate, if not, to survive. In this study, cluster stability has been estimated by using the kinetic energy of the atoms calculated in the center-of-mass system (total KE − translational KE). Indeed, it has been observed that, for sufficiently large molecules, the kinetic energy of atoms relative to the center-of-mass of the cluster at the end of the sputtering event (*a*KE in Figure 3c) was directly correlated to the total internal energy.[5] This simplified procedure bypasses the difficulty of determining the equilibrium energy of the relaxed alkanethiol clusters, which becomes a complex procedure with increasing cluster size, because of the different possible cluster conformations that give rise to local minima in the potential energy function. Using decreasing threshold values for the relative kinetic energy of the clusters, one observes that the high-energy tail of the KEDs becomes more and more depleted

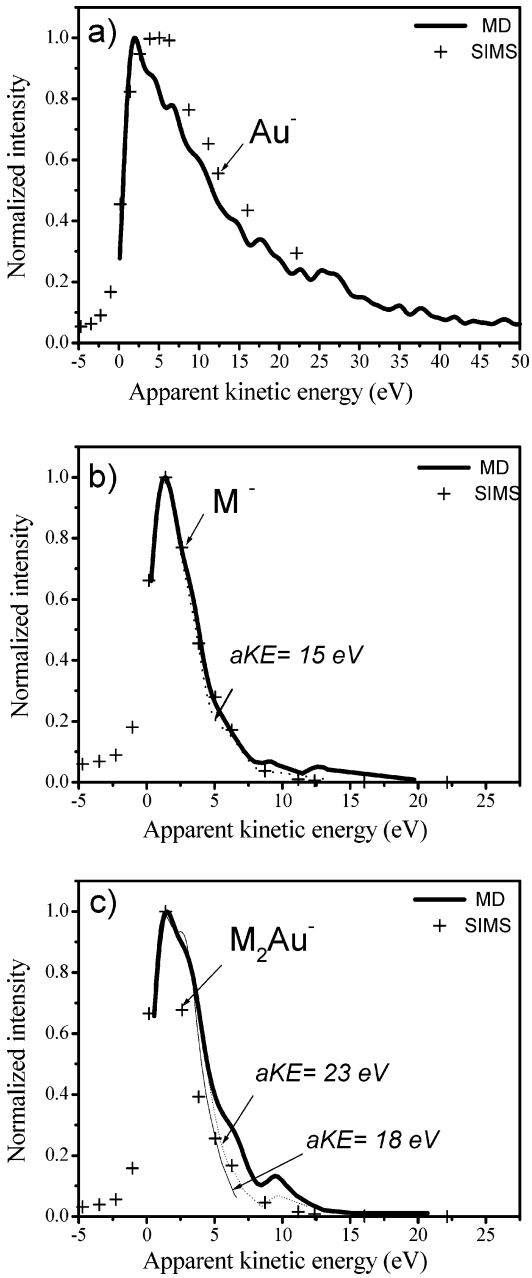

Figure 3. Kinetic energy distributions of (a) Au atoms, (b) thiolate molecules, and (c) M_2Au clusters ejected from octanethiol/Au: crosses, ToF-SIMS experiments; lines, MD simulations; dashed lines, effect of the *a*KE threshold for dissociation on the calculated KEDs (see text for details).

(Figure 3c). A threshold value of 18 eV of energy in the center-of-mass system is found to give a satisfactory agreement between MD and SIMS distributions. For an equivalent value (*a*KE = 15 eV), the distribution of the octanethiolate, M, is almost unchanged at low energy and is better fitted at high energy, above 8 eV (Figure 3b). Therefore, unimolecular dissociation processes might well be the cause of the divergence between the calculated and experimental energy distributions of Figure 3c. It should be noticed, however, that the threshold values providing the best fit are rather large considering the number of atoms in the cluster and the energy of the weakest bond.

The general agreement observed between the calculated and experimental KEDs, also observed for other systems in previous MD studies,[4,5,29] gives us the necessary confidence to interpret the details of the molecular dynamics. The straightforward

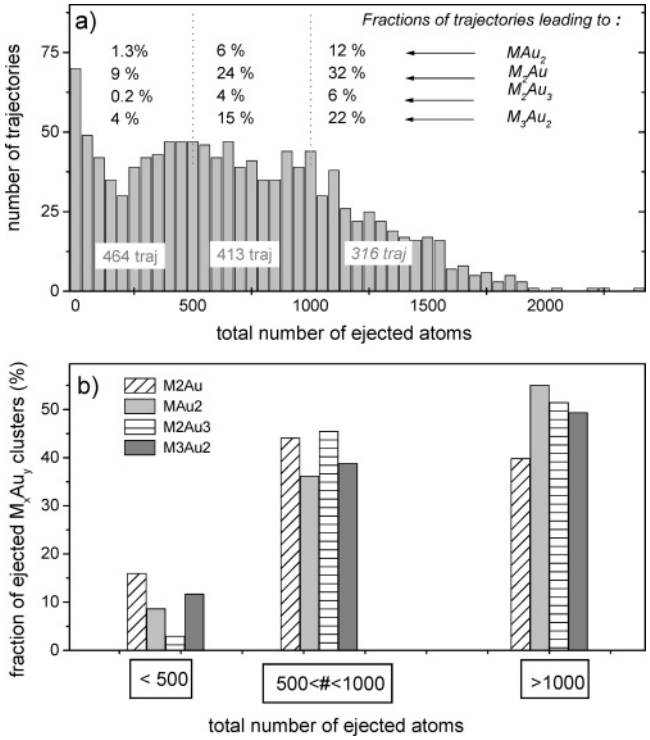

Figure 4. Statistics of the ejection events. (a) Histogram giving the number of trajectories as a function of the total number of atoms ejected in fragments and clusters. The tabulated values represent the fractions of the impacts leading to MAu_2, M_2Au, M_2Au_3, and M_3Au_2 clusters. (b) Fractions of clusters sputtered per category of ejection event.

observation of the M_xAu_y cluster energy distributions, extending up to several electronvolts, already suggests that molecule and cluster emission have a collisional origin. In the next sections, the MD results are analyzed in order to extract detailed information concerning the major scenarios of M_xAu_y cluster sputtering.

3.2. Analysis of the MD Statistics. The goal of this analysis is to determine which type of trajectory gives rise to cluster emission. For this purpose, three categories of events have been defined, as a function of the total number of atoms that are ejected in each trajectory, either as single particles or as a part of fragments and clusters. The three domains correspond to impacts emitting less than 500 atoms (I), between 500 and 1000 atoms (II), and more than 1000 atoms (III), respectively. These domains are shown in a histogram giving the number of trajectories vs the total number of ejected atoms (Figure 4a). There is a continuum of events going from low- to giant-emission yields (more than 1500 atoms). The fractions of impacts leading to MAu_2, M_2Au, M_2Au_3, and M_3Au_2 clusters help to have a more detailed view regarding the origin of some of the observed aggregates. These values are calculated with respect to the total number of trajectories in each domain. For instance, among the 464 impacts leading to less than 500 atoms in total, 9% of them give rise to M_2Au clusters, while these same clusters come from 24% among the 413 impact and 32% among the 316 impacts of domains II and III, respectively. In general, these fractions are proportional to the total number of ejected atoms. In complement, the bar graph of Figure 4b displays the fraction of the total number of these clusters sputtered for each domain. It shows that the vast majority of the considered clusters (~90%) come from high-yield trajectories, involving more than 500 ejected atoms. About half of them are sputtered in the 26% of trajectories ejecting more than 1000 atoms. The graph also indicates that all the considered

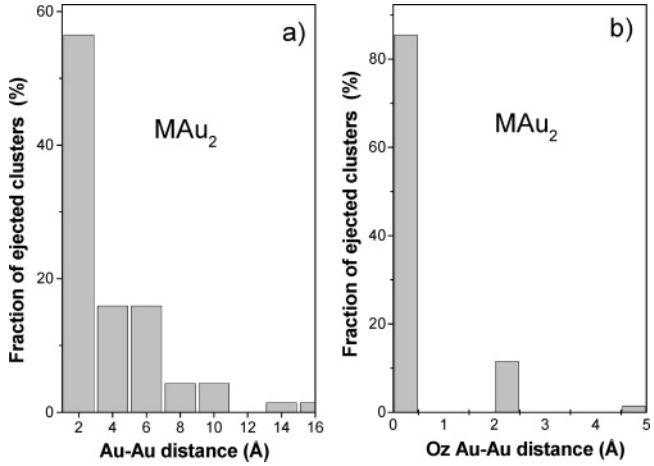

Figure 5. Total number of ejected MAu_2 clusters as a function of (a) the Au−Au distance prior to Ar bombardment and (b) the Au−Au distance along the Oz axis.

clusters follow the same trend, that is, there is no specific behavior related, for instance, to the size of the cluster.

Other questions that have been raised in previous reports concern the proximity between the constituents of a cluster prior to emission.[12] To address these questions, first, clusters containing two Au atoms (M_xAu_2) have been investigated. The Au atoms belonging to these clusters are often direct neighbors prior to Ar bombardment. More specifically, 57% (see Figure 5a) and 62% (not shown here**)** of the MAu_2 and M_2Au_2 (M_3Au_2) clusters, respectively, involve a pair of Au atoms that were at 2.8 Å from each other, that is, the shortest distance between two atoms in the relaxed gold crystal. For the same M_xAu_2 clusters, more than 85% of the Au atom pairs originate from the top gold layer (see Figure 5b for MAu_2). So, in most cases, the formation of these clusters does not involve a significant relative displacement of the substrate atoms in the crystal prior to their association. Even when there is clearly recombination in the surface region of Au atoms that were not direct neighbors (about 40% of the population, Figure 5a), the two atoms generally come from the top layer of the crystal. Second, the Au atoms involved in the ejected MAu clusters do *not* predominantly belong to the adsorption site of the corresponding thiolate. Only 12% of them originate from a distance of about 2.8 Å whereas 26% and 42% were second and third neighbors, respectively, prior to Ar bombardment (Figure 6a). This might be explained by the fact that Au−S bonds are often cleaved due to the multiple atomic motions in the subsurface region. The thiolate attaches afterward to a Au atom ejected near its adsorption site. This atom originates predominantly from the top layer (Figure 6b). Finally, the original proximity of the thiolates found in the ejected M_2Au_y aggregates has been investigated. It is found that 99% (Figure 7), 96%, and 94% of the M_2Au, M_2Au_2, and M_2Au_3 clusters, respectively, are formed by thiolates that were direct neighbors prior to impact.

Despite the difference of the projectile energies (and the different molecular sizes), these results are similar to those obtained in ref 12 for the 700 eV bombardment of a pentanethiol monolayer ($CH_3(CH_2)_4S$). Therefore, the projectile energy does not significantly influence the clustering of small gold−thiolate aggregates. This observation suggests that the emission process is not directly governed by the total energy deposited in the target but, rather, by the fraction of the projectile energy that is locally deposited in the topmost layers. It is shown in the next section that the way the energy dissipates in the sample is mainly dictated by the properties of the collision cascade. In addition,

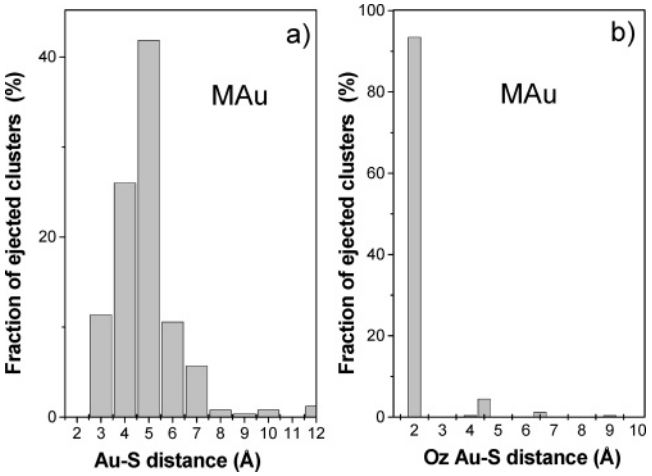

Figure 6. Total number of ejected MAu clusters as a function of (a) the Au−S distance prior to Ar bombardment and (b) the Au−S distance along the Oz axis.

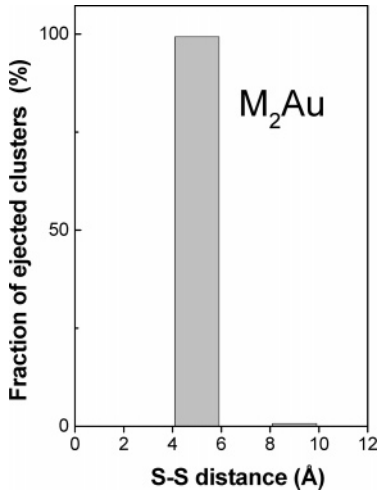

Figure 7. Total number of ejected M_2Au clusters as a function of the S−S distance prior to Ar bombardment.

our observations do not support a picture of the ejection process in which the "building blocks" of the clusters would be emitted from different regions of the sample and then recombine in the vacuum or a scenario where there would be a lot of atomic mixing in the gold crystal *prior to* cluster formation. Instead, ejection from a confined region (about 10 Å of radius), involving metal atoms from the gold−thiol interfacial layer, seems privileged under the considered bombardment conditions.

This study helped us to isolate the major categories of sputtering events and to delineate some predominant features of the cluster formation process for medium-sized species. For larger aggregates, the sputtering yields are too low to proceed to a statistically relevant analysis. On the other hand, important features of the emission process are not explained by this type of analysis. Among the 1200 calculated impacts, many specific scenarios have been observed, depending on the geometrical configuration of the primary particle impact. To illustrate some specifics of cluster emission and to gain insights into the formation mechanisms of large aggregates, not observed in previous MD studies,[10−12] the last part of the results focuses on the mechanistic description of selected trajectories.

3.3. Microscopic View of the Emission Mechanisms. In Figure 8, snapshots of the MD simulations illustrate the action occurring in two trajectories corresponding, respectively, to low-yield (trajectory L, parts a and b of Figure 8) and high-yield

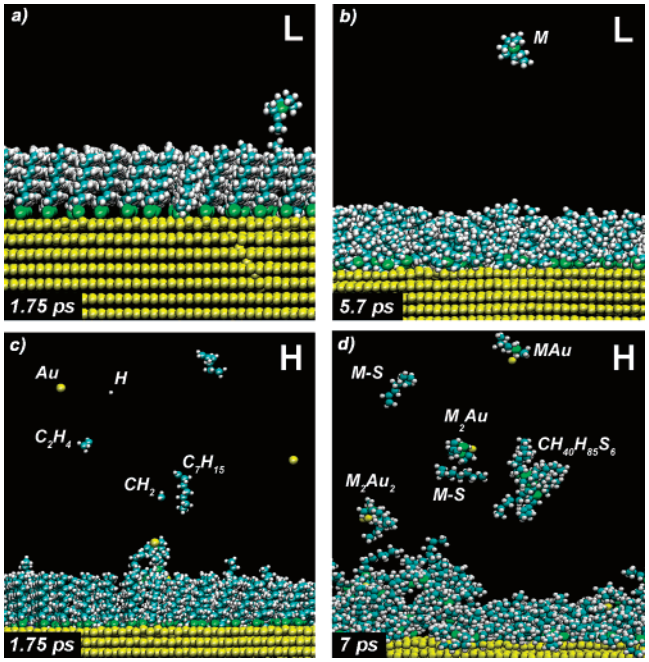

Figure 8. Temporal evolution of two trajectories leading to a low-yield (trajectory L (a and b)) and a high-yield event (trajectory H (c and d)) under 8 keV Ar bombardment of octanethiol/Au.

events (trajectory H, parts c and d of Figure 8). In trajectory L, the sputtered atoms are distributed in only two sputtered species: one Au atom (not shown) and one thiolate molecule M. The sample is left almost undamaged at the end of the trajectory. The second impact leads to the ejection of a high number of secondary species. A first batch of sputtered atoms and fragments, present at 1.75 ps after Ar bombardment, includes CH_2, C_2H_4, and C_7H_{15} (Figure 8c). Later on, at $t = 7$ ps, various molecular aggregates are observed above the surface, for example, M−S, $C_{40}H_{85}S_6$, MAu, M_2Au, and M_2Au_2 clusters (Figure 8d).

Trajectory H has been chosen to obtain mechanistic information regarding the emission of the observed M_xAu_y clusters in such a high-yield event. Parts a and b of Figure 9 display two snapshots of a cross-section through the sample to better illustrate the action in the substrate. At the early stage of the trajectory (250 fs), a few C_xH_y fragments are already ejected and the motion in the Au crystal pushes substrate atoms into the organic medium (Figure 9a). One of the Au recoils attaches to a thiolate molecule, forming a MAu cluster (yellow rectangle). After 2.5 ps (Figure 9b), the MAu cluster is far from the surface and another cluster, M_2Au_2, is desorbing from the energized region. This cluster eventually separates from the surface around 4 ps (see the inset). What the cross-sections of parts a and b of Figure 9 make particularly clear is the high action induced in the Au substrate after the penetration of the projectile. Around the entry point of the Ar atom in the crystal, many substrate atoms are simultaneously set in motion, creating a disordered region in the sample. This excited volume is responsible for the emission of the observed clusters.

To understand how the primary particle energy is transferred to the sample in the first stage of the interaction, a plot illustrating the atomic motion in the crystal over the first 200 fs is displayed in Figure 9c. This collision tree shows the successive positions of the moving substrate atoms as a function of time, that is, the spatial fingerprint of the atomic collision cascade.[30] For the sake of clarity, the plot only shows recoil atoms with more than 10 eV of kinetic energy. In addition, the

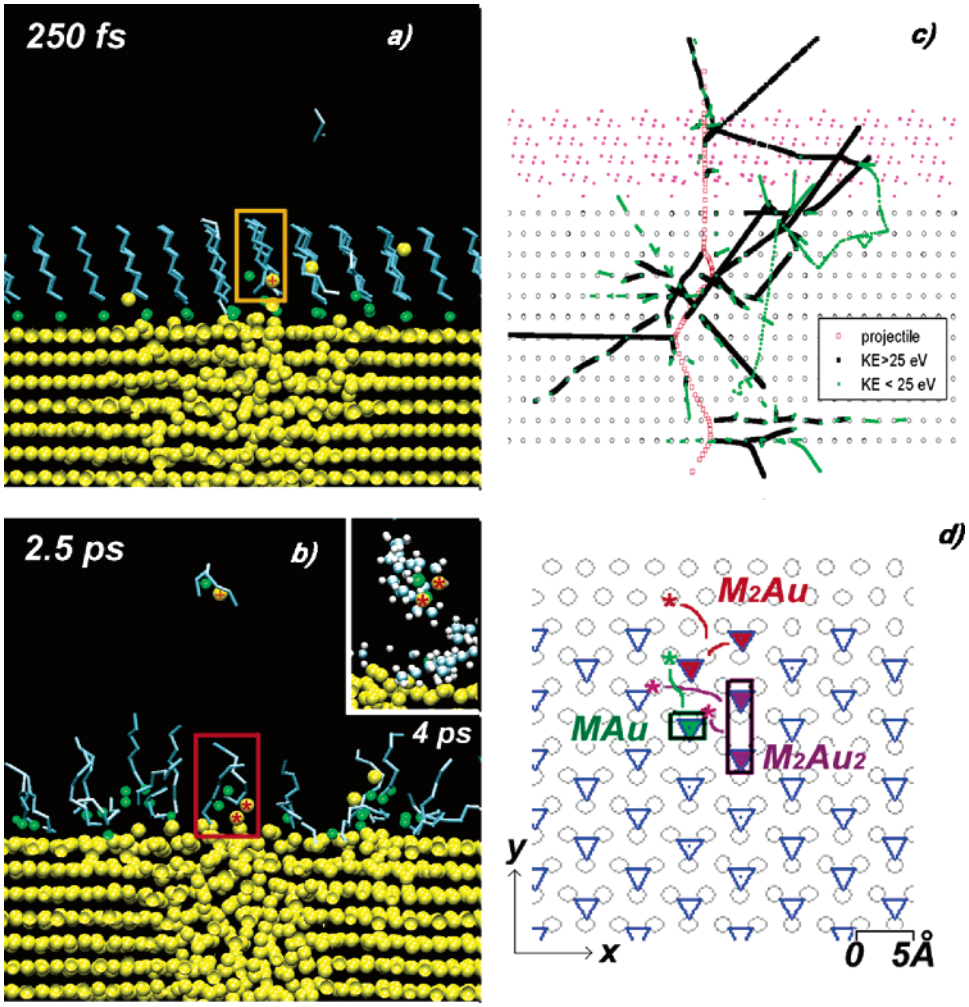

Figure 9. Mechanistic analysis of cluster sputtering. (a and b) Movie snapshots through a cross section (~10 Å) in the sample illustrating the action occurring at (a) 250 fs and (b) 2.5 ps. (c) Collision tree showing the successive positions of the moving atoms over the first 200 fs after impact. The projectile is represented by red spheres. The moving recoil atoms with KE > 25 eV and KE < 25 eV are represented by black and green dots, respectively. (d) Initial positions (prior to Ar bombardment) of the observed MAu, M_2Au, and M_2Au_2 cluster constituents. The top Au layer is represented by gray circles and S atoms by blue triangles.

Ar projectile and the recoil atoms having more or less than 25 eV are differentiated by the color code. Figure 9c shows that the projectile goes right through the entire sample, without being strongly deviated from its path by the successive collisions. It exits out of the bottom of the crystal with 4.6 keV of energy, that is, almost half of the primary particle energy is lost mainly in the gold crystal and to a lesser extent in the organic layer. This amount of deposited energy induces multiple high-energy collisions between the recoils in the middle part of the crystal. As a result of the subcascade overlapping, a high-action region is created, where many Au atoms are simultaneously set in motion. This simultaneous action is responsible for the disordered region in the topmost layers of the gold crystal. It creates a superheated volume from the surface of which clusters are ejected, as illustrated in Figure 8d and Figure 9b. The analysis of the ejection of MAu, M_2Au, and M_2Au_2 clusters shows that the associated Au atoms originate from an area that is close to the desorbed thiolates (Figure 9d), although they do not belong to the corresponding sulfur adsorption site. This is representative of the dominant scenario, as shown by the statistics of Figure 6. In fact, the recombination between the gold atoms and the thiolate molecules happen during their ejection, when they are still in the organic layer. In trajectory H, all the substrate atoms involved in aggregates originate from the first Au layer, another major characteristic of medium-sized cluster ejection. In summary, the comparison between trajectories L and H reveals two kinds of sputtering events. In the low-action event (L), molecules and/or very small clusters are pushed upward by isolated cascade atoms. In the high-action case (H), atoms and small fragments are emitted first, within the few hundreds of femtoseconds after the primary particle impact. Then, larger fragments and clusters desorb from a region where many substrate and thiol atoms are set in motion. Considering the involved energies, largely hyperthermal, the mechanism evokes more an explosion followed by an adiabatic expansion than evaporation or sublimation processes. The energetic part of the collision tree (Figure 9c) shows that the observed action is the consequence of a dense network of subcascades created in the surface region.[30]

The large M_xAu_y clusters observed under 8 keV Ar bombardment (as opposed to 700 eV bombardment[12]) arise from dramatic events that can be seen as extreme cases of the type of high-yield event unfolding in trajectory H. Such "mega-events"[6,7] do not occur below a certain threshold of projectile energy, which itself depends on the nature of the sample and the projectile. They were not observed for polystyrene adsorbates on silver under 500 eV Ar bombardment and for alkanethiol overlayers on gold bombarded by 700 eV Ar atoms.[12] For polystyrene adsorbed on silver, the energy threshold was found to be between 1.5 and 5 keV.[30] Figure 10a displays the action occurring in a mega-event induced in the gold crystal by an 8

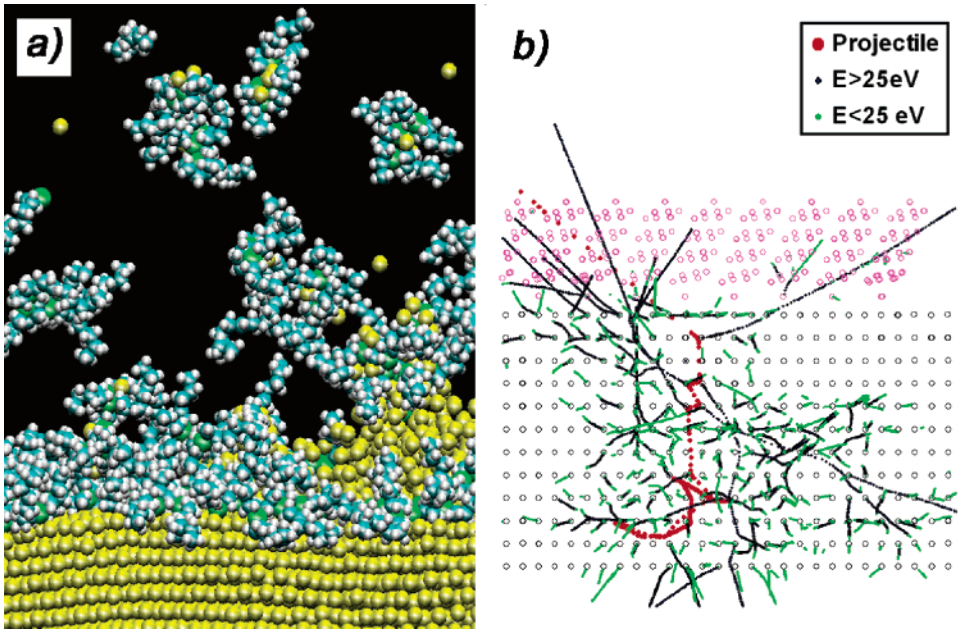

Figure 10. Dynamics of a mega-event. (a) Movie snapshot illustrating the high-action unfolding at 6 ps for a trajectory where large gold−thiolate clusters are emitted. (b) Collision tree showing the successive positions of the moving atoms over the first 200 fs after impact. The projectile is represented by red spheres. The moving recoil atoms with KE > 25 eV and KE < 25 eV are represented by black and green dots, respectively.

keV Ar projectile. After 4 ps, an important fraction of the sample surface is affected by the simultaneous motion of hundreds of substrate atoms. A protrusion of gold atoms on the right side of Figure 10a demonstrates the collective nature of the action and its scale. It appears that the largest aggregates detach from the surface as a whole, entrained by the movement of gold atoms. The collision tree of the trajectory shows that collision events essentially occur in the metal (Figure 10b). The cascade is significantly more developed than that of Figure 9c and the projectile stops in the gold crystal, that is, all of its energy (8 keV) is transferred to the target atoms. This quantity of energy corresponds to about 1 eV per gold atom of the target, that is, in terms of temperature, much more than what is needed to melt a real crystal. In practice, there are a large number of recoil atoms in a confined space (about 25 Å in diameter). They cause a disruption of the gold crystal around the path of the projectile, and a spherical hole is formed in the subsurface layers after a few picoseconds (not shown). The protrusion observed at the surface is constituted by material excluded from that expanding hole. The evolution of this trajectory (and others) after 5 ps indicates that the formation of very large agglomerates, containing more than 10 molecules, and as many gold atoms, are not rare. After ejection, they tend to dissociate into smaller entities, thereby reducing their internal energy.

4. Conclusion

The present study aimed at understanding the physical processes underlying the emission of gold−thiolate clusters from octanethiols/Au SAMs under keV ion bombardment. The general agreement between mass and energy spectra obtained from MD calculations and those measured by SIMS supports the collisional aspect of the processes involved in the sputtering of M_xAu_y clusters. Nevertheless, desorption induced by simple binary collisions is not the predominant mechanism explaining the ejection of clusters containing more than 2−3 constituents, as shown by the statistics of the desorption process and the microscopic details of specific trajectories.

The statistical study of the MD results reveals that M_xAu_y clusters are predominantly produced in high-yield events. A large percentage of M_xAu_2 aggregates consist of gold atoms that were neighbors prior to Ar bombardment and originated from the top gold layer. Also, a large majority of M_2Au_y aggregates are formed by thiolate neighbors. The dynamics and the collision trees of high-yield trajectories suggest that M_xAu_y clusters are ejected long after the development of the collision cascade, as a result of the simultaneous motion of many substrate atoms in the sample. The clusters emerge from an overheated liquidlike region, which results from the large amount of primary energy dissipated in the metal surface. The emission of the largest clusters, not observed in studies involving sub-kiloelectronvolt projectile energies, is caused by mega-events where hundreds of substrate atoms are collectively set in motion.

Acknowledgment. This work and B.A. are supported by the PAI-IUAP P4/10 research program on "Quantum effects in nanostructures", funded by the Belgian Federal State. A.D. also acknowledges the Belgian Fonds National pour la Recherche Scientifique for financial support. B.J.G. gratefully acknowledges the support of the National Science Foundation of America. Computational resources were provided by Academic Services and Emerging Technologies (ASET). The authors are also thankful to the ASET staff for assistance with the Lion-xe and Lion-xl clusters. The ToF-SIMS instrument was acquired with the support of the Région Wallonne and FRFC-Loterie Nationale of Belgium. The theoretical and computational biophysics group of the University of Illinois at Urbana-Champaign is acknowledged for the development and free access to the visualization software VMD.

References and Notes

(1) Benninghoven, A., Hunter, J. L., Schueler, B. W., Smith, H. E., Werner, H. W., Eds. *Proceedings of the 14th International Conference on Secondary Ion Mass Spectrometry, SIMS XIV*; *Appl. Surf. Sci.* **2004**, 231−232.

(2) Vickerman, J. C., Briggs, D., Eds. *ToF-SIMS: Surface Analysis by Mass Spectrometry*; SurfaceSpectra/IMP: Chichester, U.K., 2001.

(3) Sigmund, P. In *Sputtering by Particle Bombardment I*; Behrisch, R., Ed.; Springer-Verlag: Berlin, 1981; p 9.

(4) Chatterjee, R.; Postawa, Z.; Winograd, N.; Garrison, B. J. *J. Phys. Chem. B* **1999**, *103*, 151.
(5) Delcorte, A.; Vanden Eynde, X.; Bertrand, P.; Vickerman, J. C.; Garrison, B. J. *J. Phys. Chem. B* **2000**, *104*, 2673.
(6) Garrison, B. J.; Delcorte, A.; Krantzman, K. D. *Acc. Chem. Res.* **2000**, *33*, 69.
(7) Garrison, B. J. In *ToF-SIMS: Surface Analysis by Mass Spectrometry*; Vickerman J. C., Briggs, D., Eds.; SurfaceSpectra /IMP: Chichester, U.K., 2001; p 223.
(8) Delcorte, A.; Bertrand, P.; Garrison, B. J. *J. Phys. Chem. B* **2001**, *105*, 9474.
(9) Postawa, Z.; Ludwig, K.; Piaskowy, J.; Krantzman, K.; Winograd, N.; Garrison, B. J. *Nucl. Instrum. Methods Phys. Res., Sect. B* **2002**, *202*, 168.
(10) Liu, K. S. S.; Vickerman, J. C.; Garrison, B. J. *Radiat. Eff. Defects Solids* **1997**, *142*, 205.
(11) Liu, K. S. S.; Vickerman, J. C.; Garrison, B. J. In *The Proceedings of the Eleventh International Conference on Secondary Ion Mass Spectrometry (SIMS XI)*; Gillen, G., Lareau, R., Benett, J., Stevie, F., Eds.; John Wiley & Sons Ltd.: New York, 1998; p 443.
(12) Liu, K. S. S.; Yong, C. W.; Garrison, B. J.; Vickerman, J. C. *J. Phys. Chem. B* **1999**, *103*, 3195.
(13) Schreiber, F. *Prog. Surf. Sci.* **2000**, *65*, 151.
(14) Leggett, G. J. In *ToF-SIMS: Surface Analysis by Mass Spectrometry*, Vickerman, J. C., Briggs, D., Eds.; SurfaceSpectra/IMP: Chichester, U.K., 2001; p 573.
(15) Tarlov, M. J.; Newman, J. G. *Langmuir* **1992**, *8*, 1398.
(16) Rading, D.; Kersting, R.; Benninghoven, A. *J. Vac. Sci. Technol., A* **2000**, *18*, 312.
(17) Postawa, Z.; Meserole, C. A.; Cyganik, P.; Szymonska, J.; Winograd, N. *Nucl. Instrum. Methods Phys. Res., Sect. B* **2001**, *182*, 148.
(18) Wolf, K. V.; Cole, D. A.; Bernassek, S. L. *J. Phys. Chem. B* **2002**, *106*, 10382.
(19) Schroder, M.; Sohn, S.; Arlinghaus, H. F. *Appl. Surf. Sci.* **2004**, *231−232*, 164.
(20) Arezki, B.; Delcorte, A.; Bertrand, P. *Nucl. Instrum. Methods Phys. Res., Sect. B* **2002**, *193*, 755.
(21) Arezki, B.; Delcorte, A.; Chami, A. C.; Garrison, B. J.; Bertrand, P. *Nucl. Instrum. Methods Phys. Res., Sect. B* **2003**, *212*, 369.
(22) Arezki, B.; Delcorte, A.; Bertrand, P. *Appl. Surf. Sci.* **2004**, *231−232*, 122.
(23) Kelchner, C. L.; Halstead, D. M.; Perkins, L. S.; Wallace, N. M.; Depristo, A. E. *Surf. Sci.* **1994**, *31*, 425.
(24) Stuart, S. J.; Tutein, A. B.; Harrison, J. A. *J. Chem. Phys.* **2000**, *112*, 6472.
(25) Brenner, D. W.; Shenderova, O. A.; Harrison, J. A.; Stuart, S. J.; Ni, B.; Sinnott, S. B. *J. Phys: Condens. Matter* **2002**, *714*, 83.
(26) Bertrand, P.; Weng, L. T. *Mikrochim. Acta* **1996**, *13*, 167.
(27) Delcorte, A.; Bertrand, P. *Nucl. Instrum. Methods Phys. Res., Sect. B* **1996**, *115*, 246.
(28) Schueler, B. W. *Microsc. Microanal. Microstruct.* **1992**, *3*,119.
(29) Solomko, V.; Delcorte, A.; Garrison, B. J.; Bertrand, P. *Appl. Surf. Sci*. **2004**, *231−232*, 48.
(30) Delcorte, A.; Garrison, B. J. *J. Phys. Chem. B* **2000**, *104*, 6785.